Published in final edited form as:

Mol Reprod Dev. 2019 May ; 86(5): 543–557. doi:10.1002/mrd.23131.

Disruption of O-GlcNAc homeostasis during mammalian oocyte meiotic maturation impacts fertilization

Luhan T. Zhou[1], **Raquel Romar**[2], **Mary Ellen Pavone**[1], **Cristina Soriano-Úbeda**[2], **John Zhang**[1], **Chad Slawson**[3], and **Francesca E. Duncan**[1,*]

[1]Department of Obstetrics and Gynecology, Feinberg School of Medicine, Northwestern University, Chicago, IL,

[2]Department of Physiology, Faculty of Veterinary Science, University of Murcia, Spain,

[3]Department of Biochemistry and Molecular Biology, University of Kansas Medical School, Kansas City, KS

Abstract

Meiotic maturation and fertilization are metabolically demanding processes, and thus the mammalian oocyte is highly susceptible to changes in nutrient availability. O-GlcNAcylation – the addition of a single sugar residue (O-linked β-N-acetylglucosamine) on proteins - is a post-translational modification (PTM) that acts as a cellular nutrient sensor and likely modulates the function of oocyte proteins. O-GlcNAcylation is mediated by O-GlcNAc transferase (OGT) which adds O-GlcNAc onto proteins and O-GlcNAcase (OGA) which removes it. Here we investigated O-GlcNAcylation dynamics in bovine and human oocytes during meiosis and determined the developmental sequelae of its perturbation. OGA, OGT, and multiple O-GlcNAcylated proteins were expressed in bovine cumulus oocyte complexes (COCs), and they were localized throughout the gamete but were also enriched at specific subcellular sites. O-GlcNAcylated proteins were concentrated at the nuclear envelope at prophase I, OGA at the cortex throughout meiosis, and OGT at the meiotic spindles. These expression patterns were evolutionarily conserved in human oocytes. To examine O-GlcNAc function, we disrupted O-GlcNAc cycling during meiotic maturation in bovine COCs using Thiamet-G (TMG), a highly selective OGA inhibitor. Although TMG resulted in a dramatic increase in O-GlcNAcylated substrates in both cumulus cells and the oocyte, there was no effect on cumulus expansion or meiotic progression. However, zygote development was significantly compromised following in vitro fertilization (IVF) of COCs matured in TMG due to effects on sperm penetration, sperm head decondensation, and pronuclear formation. Thus, proper O-GlcNAc homeostasis during meiotic maturation is important for fertilization and pronuclear stage development.

Keywords

O-GlcNAc; oocyte; meiotic maturation; fertilization; mammalian

[*]**Correspondence:** Francesca E. Duncan, PhD, Department of Obstetrics and Gynecology, Feinberg School of Medicine, Northwestern University, 303 E. Superior Street, Lurie 7-117, Chicago, IL 60611, Tel: 312-503-2172, f-duncan@northwestern.edu.

Conflict of Interest

The authors have no conflict of interest to disclose.

Introduction

During development, the mammalian oocyte is one of the most transcriptionally and translationally active cells in the body leading to tremendous volumetric expansion (Gosden and Lee 2010). The high amount of protein synthesis and size expansion places the oocyte under a high energetic demand (Gu et al. 2015). To accommodate the high energetic demand, oocytes are supported by somatic granulosa cells that nurture the oocyte through bidirectional communication and metabolic cooperativity (Eppig et al. 2005; Russell et al. 2016). The granulosa cells provide the oocyte with nutrients, metabolic precursors, growth factors, and hormones to regulate oocyte growth and development, transcriptional activity, and meiotic progression. In turn, the oocyte produces secreted factors that regulate granulosa cell proliferation, differentiation and function (Eppig et al. 2005; Russell et al. 2016). However, oocyte-granulosa cooperativity is highly sensitive to conditions of altered metabolism such as obesity, diabetes, metabolic syndrome, and polycystic ovarian syndrome – all of which are associated with poor gamete quality and adverse reproductive outcomes (Dumesic et al. 2008; Purcell and Moley 2011; Wang and Moley 2010). Importantly, excess nutrients from “Western Diets” are contributing to the rise in metabolic syndromes in women of reproductive age; thus, a critical understanding as to how metabolic pathways regulate oocyte development and quality is needed.

The highly conserved hexosamine biosynthetic pathway (HBP) metabolic pathway links nutrient flux and cell signaling (Hart 2014; Olivier-Van Stichelen and Hanover 2015). This pathway accounts for between 2–5% of total cellular glucose metabolism within a cell while also integrating amino acid, fatty acid, and nucleotide metabolism to generate the final product of this pathway: uridine diphosphate N-acetylglucosamine (UDP-GlcNAc) (Hardiville and Hart 2014). UDP-GlcNAc is then either incorporated into proteoglycans and glycosaminoglycans or it is utilized as the substrate for the post-translational modification of proteins via O-GlcNAcylation – the attachment of a single N-acetyl glucosamine moiety (O-GlcNAc) to serine and threonine (S/T) residues of nuclear, cytoplasmic, and mitochondrial proteins (Hart 2014). Previously, glucosamine, which bypasses the rate limiting enzyme of the HBP and leads to increased UDP-GlcNAc levels, has been used to mimic hyperglycemic conditions in mouse, bovine, and porcine cumulus oocyte complexes (COCs) (Frank et al. 2014a; Pantaleon et al. 2010; Sutton-McDowall et al. 2006). Exposure of COCs to glucosamine during in vitro maturation (IVM) significantly compromises the developmental competence of the resulting gametes demonstrating the negative consequences of the hyperglycemic environment (Frank et al. 2014b; Wong et al. 2015). Although glucosamine is an important tool for stimulating the HBP, this treatment induces a pathological condition and it remains unclear whether the observed phenotypes in glucosamine-treated COCs are due specifically to downstream effects on proteoglycans and glycosaminoglycans and/or on the process of O-GlcNAcylation.

Due to the sensitivity of the O-GlcNAcylation reaction toward UDP-GlcNAc levels and the transient nature of the modification, O-GlcNAc is considered a cellular sensor of nutrient status (Bond and Hanover 2015; Hardiville and Hart 2014; Olivier-Van Stichelen and Hanover 2015). O-GlcNAcylation regulates numerous physiologic processes, and the

cycling of O-GlcNAc on and off proteins is mediated by only two enzymes. O-GlcNAc transferase (OGT) catalyzes the addition of UDP-GlcNAc onto proteins to form a β-glycosidic linkage. In contrast, O-GlcNAcase (OGA) removes the modification (Hart 2014). Dynamic cycling of O-GlcNAc on and off proteins is necessary for normal development. In fact, deletion of OGT is lethal in mice and flies, and knocking out OGT in cultured cells leads to growth senescence and apoptosis (Janetzko and Walker 2014). OGA knockout mice have severe growth defects, binucleated cells, and chromosomal abnormalities and die as neonates (Alonso et al. 2014). Together, these data demonstrate an essential role for O-GlcNAc cycling in regulating cell growth and division.

Given that O-GlcNAcylation is a nutrient sensor modulating cellular homeostasis, we hypothesized that O-GlcNAc would have an essential role during mammalian oocyte development, and we interrogated this post-translational modification (PTM) in both bovine and human oocytes. Under physiologic conditions, OGA, OGT, and O-GlcNAcylated proteins were expressed in oocytes and cumulus cells, and these proteins underwent dynamic changes during meiotic maturation. Using an OGA inhibitor to specifically target O-GlcNAc turnover, we induced a hyper-O-GlcNAcylated state in the oocyte and cumulus cells downstream of proteoglycan and glycosaminoglycan modulation. While this increase in protein O-GlcNAcylation did not affect meiotic progression, it did dramatically compromise fertilization and zygote development. Thus, proper O-GlcNAc homeostasis is essential for the developmental potential of the oocyte.

Materials and Methods

Source of bovine ovaries

Cumulus oocyte complexes used in this study were collected from ovaries harvested at two different locations. The majority of the experiments described in this study were performed in Illinois, and bovine ovaries were obtained from Aurora Packing Company (Aurora, IL) and transported by courier service to Northwestern University within two hours of harvest. The Aurora Packing Company is a slaughterhouse that processes cattle from multiple sites across the Midwest within a 300 mile radius of Chicago. Although we did not have control over the source of the material we received from Aurora Packing Company, they primarily process beef cattle (Angus breed), and the heifers were post-pubertal and reproductively adult (between 24 to 30 months). The experiments performed in Spain (Table 1 and Figure 8) used ovaries from slaughterhouses that received animals from specific farms with the following breeds: Limousin, Simmenthal and Charolaise, and some beef cattle such as Blonde d'Aquitaine. These animals were approximately 12–18 months of age. Although it is possible that these differences in age and breed could have introduced variability in our data, within any given experiment, control and experimental cohorts of oocytes were from the same source of ovaries and were compared in parallel.

Collection of bovine cumulus oocyte complexes, in vitro maturation (IVM), and cumulus cell isolation

Cumulus oocyte complexes (COCs) were isolated from whole ovaries by slashing small antral follicles (3–9 mm) with a scalpel directly into 1X Leibovitz's medium (L15) (Life

Technologies Corporation, Grand Island, NY) containing 3 mg/ml polyvinylpyrrolidone (PVP) (Sigma-Aldrich, St. Louis, MO) and 0.5% Pen Strep (Life Technologies) (L15/PVP/PS). This medium was then passed through a 100 μm mesh filter to capture the COCs, which were then rinsed off and recovered from the filter. Only morphologically healthy COCs were selected for either immediate examination of the germinal vesicle (GV) stage or for in vitro maturation (IVM) to obtain mature eggs at metaphase of meiosis II (MII). We selected COCs that had at least 3–5 layers of dense cumulus cells surrounding a round oocyte that had a dark but uniform lipid rich cytoplasm. COCs with translucent or dark cumulus cells or partially denuded COCs were avoided as were completely denuded oocytes. For IVM, 15–25 COCs were transferred to BoviPRO Oocyte Shipping and Maturation Media (19982/1231, MOFA, Verona, WI). The medium was overlaid with 500 μl of mineral oil (Sigma-Aldrich) and cultured at 39°C for 22–24 hours as this is the time point at which most oocytes reach the mature MII-arrested state (Ward et al. 2002). Following IVM, COCs were removed from each vial, and when relevant, cumulus cells were denuded by mechanical disruption with the addition of 1 μM hyaluronidase (Sigma-Aldrich). The hyaluronidase was then removed by rinsing through large drops of L15/PVP/PS. Transmitted light images were taken on an EVOS FL Auto Cell Imaging System (ThermoFisher Scientific, Waltham, MA) using 10X, 20X, and 40X objectives. Following collection, COCs, denuded oocytes, and cumulus cells were either snap frozen or fixed and processed as described below.

Human oocyte acquisition

Immature human oocytes that would otherwise be discarded from Assisted Reproductive Technology (ART) cycles were acquired through the Reproductive Tissue Library at Northwestern University (NU-RTL). The NU-RTL is an Institutional Review Board-approved study in which participants can elect to donate discarded reproductive tissues, cells, and fluids for research purposes following informed consent. These oocytes were obtained from participants on the day of scheduled oocyte retrieval. Following retrieval, the cumulus cells were removed from the oocyte in the clinic, and the meiotic status of the gamete was assessed by morphology. Immature oocytes, which would otherwise be discarded, were donated to the NU-RTL and delivered to the research laboratory within a maximum of 6 hours post-retrieval. By the time the oocytes reached the research laboratory, they were at various stages of meiotic progression, which was assessed by morphology and transmitted light microscopy. In brief, the presence of a germinal vesicle at Prophase I was scored as GV stage, absence of the germinal vesicle with the absence of the polar body (PB) was scored as prometaphase/metaphase of Meiosis I (GVBD/MI stage), and the presence of a PB was scored as metaphase of Meiosis II (MII stage). Upon receipt, oocytes were imaged, either snap frozen or fixed, and processed further as described below.

Antibodies

The anti-O-linked N-acetylglucosamine antibody (RL2) (MA1–072) was purchased from ThermoFisher Scientific, and the anti-O-GlcNAcase (OGA) antibody produced in rabbit (SAB4200311) was purchased from Sigma Aldrich. The anti-OGT (AL-35, AL-28) and OGA (AL-345) antibodies were rabbit and chicken polyclonal antibodies, respectively, and were gracious gifts from the Laboratory of Gerald Hart in the Department of Biological Chemistry at the Johns Hopkins University School of Medicine. These antibodies have been

used extensively to characterize the O-GlcNAc network in several model systems (Lanza et al. 2016; Slawson et al. 2008; Slawson et al. 2005; Tan et al. 2013; Wang et al. 2010). Rabbit IgG (I-1000) and mouse IgG (I-2000) were used as negative controls (Vector Laboratories, Burlingame, CA). The MSY2 antibody was a generous gift from Richard Schultz at the University of Pennsylvania. The Alexa Fluor® 488 goat anti-mouse IgG (A-11001) and Alexa Fluor® 488 goat anti-rabbit IgG (A-11008) secondary antibodies were purchased from ThermoFisher Scientific. The donkey anti-rabbit IgG horseradish peroxidase (HRP) (NA934) and sheep anti-mouse IgG HRP (NA931) secondary antibodies were purchased from GE Healthcare. The rabbit anti-chicken IgY (IgG) HRP (A9046) secondary antibody was purchased from Sigma-Aldrich.

Immunoblotting

Previously snap frozen intact bovine COCs, denuded bovine oocytes, or denuded human oocytes were thawed, and protein extracts were separated on 4–15% gradient SDS-PAGE gels (Bio-Rad, Hercules, CA) according to standard procedure. Where relevant, controls included HeLa cell extracts (Slawson et al. 2005) or liver extracts from wild type or OGT knock-out mice (Tan et al. 2017b). Proteins were transferred onto Amersham Hybond P 0.45 PVDF membranes (GE Healthcare Life Sciences, Pittsburg, PA). To detect O-GlcNAcylated substrates, blots were blocked in 3% Amersham ECL Blocking Agent (GE Healthcare Life Sciences) diluted in Tris buffered saline containing 0.1% V/V Tween-20 (TBS-T) (block) for 3–4 hours at room temperature. Blots were then probed with RL2 diluted in 3% bovine serum albumin (BSA, Life Technologies) diluted (1:500–1:1000) in TBS-T overnight at 4°C. Blots were then rinsed three times and incubated in anti-mouse IgG HRP diluted (1:10,000) in 3% block for 1 hour at room temperature. Following secondary antibody incubations, the blots were washed 3 × 30 minutes in TBS-T and finally developed with the chemiluminescent substrate, ECL Prime (GE Healthcare) according to the manufacturer's instructions. To detect OGT, AL-35 (1:500 –1:1000) was used, to detect OGA, rabbit (1:1000) and chicken (1:1000) polyclonal antibodies were used. The MSY2 antibody to confirm oocyte loading was used at a 1:2500 dilution. OGA and OGT immunoblots were probed and developed similarly to the methods described for O-GlcNAc with the following modifications: all primary antibodies were diluted in 3% block, and secondary antibodies were anti-rabbit IgG (1:10,000) or anti-chicken IgG HRP (1:10,000). To assess protein loading, membranes were rinsed and stained using SWIFT total protein stain according to the manufacturer's instructions (G-Biosciences, St. Louis, MO). All immunoblots were repeated a minimum of three times with independent biological replicates.

Whole mount immunocytochemistry and confocal microscopy

To detect O-GlcNAcylated substrates, OGA, and OGT, denuded oocytes or cumulus cells were fixed in 3.8% paraformaldehyde for 1 hour at room temperature. Oocytes or cumulus cells were rinsed briefly in phosphate buffered saline (PBS) containing 0.3% albumin (BSA), 0.01% Tween-20, and 0.02% NaN_3 (blocking buffer), then permeabilized for 15 minutes in PBS containing 0.3% BSA, 0.1% Triton X-100, and 0.02% NaN_3 (permeabilization buffer). Cumulus cells or oocytes were then incubated in primary antibodies diluted in blocking buffer overnight at 4°C (RL2 1:100; stock: 0.3 μg/ml, rabbit OGA 1:100; stock: 1.5 μg/ml, and AL-28 1:100; stock: 2.0 μg/ml). As negative controls,

immunocytochemistry was performed with rabbit and mouse IgGs at the same concentrations as the primary antibodies. Immunocytochemistry was also performed with the primary antibody omitted (secondary antibody only) as another negative control. Cells were rinsed in blocking buffer three times, and then incubated in the appropriate secondary antibodies diluted in blocking buffer (1:100, goat anti-mouse or goat anti-rabbit AlexaFluor 488, Life Technologies) for 1 hour at room temperature. Rhodamine-phalloidin (R415, Life Technologies) was added during the secondary antibody incubation at a 1:50 dilution to detect filamentous actin. Cells were then rinsed again in blocking buffer three times and mounted in Vectashield containing DAPI (4',6-diamidino-2-phenylindole; Vector Laboratories). Cells were imaged on a Leica SP5 inverted laser scanning confocal microscope (Leica Microsystems) using 405 nm, 488 nm, and 543 nm lasers. The image acquisition parameters were set to highlight localization, and settings were determined by the glow over LUT to ensure that there was no pixel saturation. Moreover, signal specificity was confirmed with the appropriate negative controls, including both relevant non-immune IgG and no primary antibody (Supplemental Figure 1). Optical sections were taken every 1 μm, and either single sections or z-projections are shown as noted. Images were processed using LAS AF (Leica Microsystems) and Image J (National Institutes of Health, Bethesda, MD).

Thiamet-G treatment and meiotic progression

To increase O-GlcNAcylation, COCs were treated with Thiamet-G (TMG, SDChemMolecules LLC, Owings Mills, MD), a water-soluble OGA inhibitor that was synthesized based on rationale design (Yuzwa et al. 2008). TMG was resuspended in 10 mM Tris pH 7.4 at a stock concentration of 20 mM. TMG was added to media at final concentrations of 50 μM and 100 μM and incubated for either 2 or 24 hours, since these concentrations have been used previously to increase O-GlcNAcylation in cell lines (Yuzwa et al. 2008). Untreated COCs served as a control. For IVM experiments, COCs were incubated in 50 μM TMG for a total of 24 hours. Following TMG treatment and IVM, transmitted light images were taken on the EVOS FL Auto Cell Imaging System. Following this, COCs or denuded oocytes were snap frozen for immunoblot analysis as described above. To score meiotic progression, COCs were denuded post-IVM, fixed as described above, and stained with Phalloidin and DAPI. These oocytes were imaged by confocal microscopy and meiotic progression was scored based on chromatin morphology. In brief, oocytes with a visible nucleus were arrested at prophase I in the GV-intact stage. Oocytes without a nucleus or a polar body were arrested at prometaphase (GVBD) and were at MI if the chromatin was aligned tightly along the metaphase plate. Finally, cells were arrested at MII if the DNA within the oocyte was aligned along the metaphase plate and there was a polar body containing chromatin in the perivitelline space.

Bovine in vitro fertilization and fertilization analysis

In vitro fertilization studies and fertilization analyses were performed at the Department of Physiology at the University of Murcia, Spain. Ovaries were obtained from post-pubertal heifers (between 12 to 18 months) from the Matadero Orihuela S.A abattoir (Orihuela, Alicante, Spain), transported to the laboratory within 2 hours, and COCs were aspirated from 3–9 mm size follicles. Following isolation, only morphologically healthy COCs were

selected for IVM to obtain mature MII eggs. For IVM, COCs were matured as described above either supplemented with or without 50 μM TMG for 22 hours. Following IVM, COCs were thoroughly rinsed to remove any residual TMG. IVF was performed as previously described (Mondejar et al. 2012). Briefly, straws containing frozen ejaculated semen from a single Asturiana valley bull (SERIDA, Gijón, Spain) were thawed in a water bath (37°C, 1 min) and centrifuged for 5 min at 280 g in Sp-TALP (Parrish et al. 1988). Spermatozoa (1×10^6 cells/ml) were co-incubated with the COCs following IVM for 18 hours in Fert-TALP supplemented with 10 mg/mL heparin sodium salt in a four-well dish (Parrish et al. 1988). Groups of 35–40 inseminated COCs were cultured per well in a humidified atmosphere of 5% CO_2 in air at 38.5°C. Eighteen hours post-insemination, zygotes were fixed with 0.5% (v/v) glutaraldehyde (30 min, RT) and stained with 1% (w/v) Hoechst 33342 followed by imaging under epifluorescence using a 40X objective (Leica Microsystems) to assess sperm penetration (Table 1). Sperm penetration was scored when at least one spermatozoon was found within the ooplasm. Once a sperm enters the ooplasm, DNA decondensation gradually begins until the male pronucleus is formed. The sperm head can be i) compact (no signs of nuclear expansion is observed, and sperm cells maintain their paddle-shape); ii) partially decondensed (the sperm head swells and loses its typical shape but does not reach the completely spherical shape of a male pronucleus); iii) fully decondensed forming a male pronucleus (a completely spherical shape with a pronuclear envelope is observed). These are all normal configurations and represent a developmental continuum. With Hoechst staining it is not possible to distinguish between male and female pronuclei because the sperm tail is not stained. Thus, when zygotes were stained with Hoechst and two pronuclei were observed, it was assumed that one was the female and the other was the male pronucleus. In the case that only one pronucleus was observed, and no metaphase or chromatin structures from the oocyte nucleus were visible, then it is considered to be a female pronucleus and the oocyte was activated. In our experience, it is extremely rare to observe the oocyte metaphase plate together with a fully formed male pronucleus after insemination. Therefore, in this study, the variable MPNf (male pronucleus formation) referred to those zygotes that had at least 2 pronuclei, and the total number of spermatozoa per penetrated oocyte (SPZ/OO) included both the number of MPN and decondensed heads. For example, in Table 1, the total number of spermatozoa per penetrated oocytes in the control group was 1.41 (1.16 of which were MPN/OO and 0.24 decondensed SPZ/OO). Zygotes showing only two pronuclei were considered to be monospermic. The final efficiency of IVF (% output) was reported as the number of monospermic zygotes per the total number of inseminated oocytes.

Statistical analysis

Significant changes between groups were analyzed by one-way ANOVA or two-way ANOVA followed by multiple comparisons test (Tukey post hoc test). P values < 0.05 were considered statistically significant. Statistical analysis was performed using Graphpad-Prism Software Version 6.0f (La Jolla, CA).

Results

The O-GlcNAc regulatory machinery and O-GlcNAcylated proteins are expressed in bovine COCs

To investigate whether the O-GlcNAc regulatory machinery is expressed in bovine COCs, we performed immunoblot analysis of protein extracts with specific antibodies against OGT and OGA. OGT is a 110 kDa protein, and we detected a predominant immunoreactive band at this molecular weight in bovine COCs (Figure 1A). We also observed an additional band that ran at a lower molecular weight, but this was not observed consistently and thus this band is likely a degradation product (Figure 1A). The OGT antibody is specific because it recognizes an immunoreactive band of the correct molecular weight in control HeLa cell lysates (Figures 1A–B). Moreover, as an additional control, we ran liver extract lysates from wild type and knockout OGT mice and found that the immunoreactive band was present in wild type but not in knockout liver extracts when equal amounts of protein were loaded as assessed by the SWIFT total protein stain (Figure 1B; right panel). OGA is a 120 kDa protein, and we detected a predominant immunoreactive band of at this molecular weight in bovine COC extracts (Figure 1C–D). Because we did not have access to protein extracts from OGA knockout tissues, we instead used two different independent antibodies (mouse and rabbit) raised against the OGA to demonstrate that the immunoreacitve band is specific because both antibodies detected the same band (Figure 1C–D). This was further confirmed because the MW in the bovine COCs was the same as that detected in HeLa cell lysate, which served as a positive control because these cells are known to express OGA (Figures 1C–D). Taken together, these results demonstrate that the O-GlcNAc regulatory machinery is expressed in bovine COCs and confirm the specificity of our antibodies.

To examine whether O-GlcNAcylated proteins are present in bovine COCs, we performed an immunoblot with COC protein extracts using an antibody that recognizes the O-GlcNAc modification. We consistently observed six immunoreactive bands across replicates corresponding to O-GlcNAcylated proteins of >250, 250, 200, 150, 110, and 70 kDa, but the identity of these modified proteins has not yet been determined (Figure 1E). COCs are comprised of two cell types – the oocyte and the supporting cumulus cells that surround the oocyte (Figure 1F). To determine whether O-GlcNAcylated substrates were present in both cell types, we ran immunoblots on protein extracts from equal numbers of intact COCs and denuded oocytes that had been stripped of cumulus cells (Figures 1F–G). In this case, the signal from the intact COCs was much more intense than in the denuded oocytes because COCs are comprised of hundreds of cumulus cells in addition to the oocyte, and this is also reflected in the increased amount of total protein visible in the intact COCs versus denuded oocytes (Figure 1G). Thus, the portion of the blot containing the COC extract had to be overexposed before any signal was seen in the lane containing the denuded oocyte protein extract (Figure 1G). Although we could not make any conclusions about the relative quantity of O-GlcNAcylated substrates in the oocyte versus the cumulus cells on a per cell basis, these results nevertheless highlight that O-GlcNAcylated substrates are clearly in both the germ and somatic cell compartments of the COC (Figure 1G).

The O-GlcNAc regulatory machinery and O-GlcNAcylated proteins localize to distinct subcellular regions in bovine oocytes and cumulus cells.

To examine the subcellular distribution of the O-GlcNAc regulatory machinery in bovine oocytes, we performed immunocytochemistry and confocal microscopy with antibodies specific against OGT and OGA at two stages of meiosis: prophase I (germinal vesicle; GV-intact) and metaphase of Meiosis II (MII) (Figure 2A). We first confirmed signal specificity with the appropriate negative controls, and the fluorescence signals were essentially abrogated in the non-immune IgG and no primary antibody controls when the samples were imaged with the same settings as those used to detect the antigen of interest (Supplemental Figure 1). OGT exhibited three localization patterns in GV-intact oocytes (Figure 2B). In 42.9% of the oocytes, OGT expression was enriched in the cytoplasm, in 20.0% it was enriched in the nucleus, and in 37.1% it was distributed uniformly throughout the oocyte. Following meiotic maturation, OGT localized throughout the cytoplasm but was highly concentrated at the meiotic spindle (Figure 2B). OGA had similar expression patterns as OGT in the GV oocyte, with 45.9% of the oocytes displaying cytoplasmic enrichment, 29.7% displaying nuclear enrichment, and the remaining cells having a uniform distribution (Figure 2B). However, unlike OGT, OGA was found to be slightly more concentrated at the cortex (Figure 2B). At MII, OGA localized within the cytoplasm but was enriched at the cortex and localized to the transzonal projections that connect the oocyte with its surrounding cumulus cells (Figure 2B). To investigate the subcellular distribution of O-GlcNAcylated substrates in oocytes at different stages of meiosis, we performed immunocytochemistry and confocal microscopy with an antibody specific against the O-GlcNAc modification (Figure 2C), and antibody specificity was confirmed with relevant controls (Supplemental Figure 1). At the GV stage, the nuclear envelope was the most prominent structure containing O-GlcNAcylated substrates (Figure 2C). However, z-stack projections also revealed that O-GlcNAcylated substrates localized throughout the nucleus and cytoplasm (Supplemental Figure 2). At the MII stage, the majority of O-GlcNAcylated substrates were cytoplasmic with slight enrichment at the cortex (Figure 2C).

Based on our immunoblot findings, it is clear that cumulus cells express O-GlcNAcylated substrates (Figure 1G). To characterize the subcellular localization of the O-GlcNAc machinery and O-GlcNAcylated proteins in cumulus cells, immunocytochemistry and confocal microscopy was performed on cumulus cells isolated from COCs immediately upon collection from antral follicles. OGA, OGT, and O-GlcNAcylated proteins had dynamic localization patterns within the cumulus cells, with some cells having a uniform staining patterns while others having strong nuclear or cytoplasmic staining for these particular proteins (Figure 3). Similar to GV intact oocytes, O-GlcNAcylated proteins was also observed at the nuclear envelope in cumulus cells (Figure 3C). Taken together, these results demonstrate that O-GlcNAcylation is a prominent and dynamic protein modification in both the germ cell and somatic cell compartments of the bovine COC.

The O-GlcNAc regulatory machinery and O-GlcNAcylated proteins are conserved in human oocytes

To determine whether O-GlcNAcylation is an evolutionarily conserved modification in oocytes from large mammalian species, we examined the expression of the O-GlcNAc

regulatory machinery as well as O-GlcNAcylated proteins in human eggs (Figure 4). Of the oocytes obtained for this study, 78.5% were morphologically normal upon arrival to the lab and 21.5% were degenerate. Of the healthy cells, 58% were arrested in prophase of Meiosis I (GV), 35.3% were between GVBD and MI, and 6.7% had reached the MII stage (Figure 4A). The availability of human oocytes for research purposes is limited, but we nevertheless were able to obtain sufficient material to perform a western blot to examine O-GlcNAcylated proteins in GV-intact oocytes (Figure 4B). Although it was difficult to resolve the precise molecular weights of individual proteins, O-GlcNAc modified proteins are expressed in the human oocyte perhaps at lower levels relative to the bovine where immunoblot signals were readily obtained (Figure 4B). We also performed immunocytochemistry and confocal microscopy on human oocytes at different stages of meiosis using specific antibodies against OGT, OGA, and the modification itself (Figure 4C). OGT was cytoplasmic at all meiotic stages but had a prominent localization at both the MI and MII meiotic spindles (Figures 4C). Across all meiotic stages, OGA was concentrated at the cortex (Figures 4C). In examining the modification, itself, we observed that in GV stage oocytes, O-GlcNAcylated substrates were in the cytoplasm and enriched both at the nuclear envelope and the cortex (Figure 4C). In MI stage oocytes the modification was found to be cytoplasmic, as well as slightly enriched at the cortex (Figure 4C). Finally, in MII eggs the modification was primarily cytoplasmic (Figure 4C). These distinct subcellular localizations are consistent with what we observed in bovine, suggesting a high degree of conservation of this protein modification across mammalian species (Figure 2).

OGA inhibition perturbs O-GlcNAcylation in bovine COCs and denuded oocytes

To examine the function of O-GlcNAcylation during meiotic maturation, we disrupted O-GlcNAc cycling using Thiamet-G (TMG), a highly selective and water-soluble inhibitor of OGA. TMG treatment in several human cell lines increases levels of O-GlcNAcylated proteins (Zhang et al. 2014). To determine whether TMG treatment could perturb O-GlcNAc levels in bovine COCs and oocytes, we *in vitro* matured bovine COCs in the presence or absence of TMG and then analyzed levels of O-GlcNAcylated proteins. A short term (2 hr) exposure of intact COCs to 0 μM, 50 μM, and 100 μM TMG did not affect their morphology as assessed by light microscopy indicating that the treatment was not toxic to the cells (Figure 5A). However, none of the TMG concentrations increased levels of O-GlcNAcylated substrates during this short-term treatment (Figure 5B). We, therefore, increased the exposure time and performed IVM in the presence or absence of 50 03BCM TMG (Figure 6). This long-term exposure (22–24 hrs) to TMG during IVM did not affect the morphology of the COCs or the degree of cumulus cell expansion, suggesting that this treatment paradigm also was not overtly toxic to the COCs (Figure 6A). Following IVM, we performed immunoblot analysis of COC protein extracts to examine how TMG treatment affected the expression of O-GlcNAcylated substrates. We observed a consistent increase in O-GlcNAcylated substrates following TMG treatment relative to untreated controls (Figure 6B). To examine whether TMG treatment of intact COCs during IVM had an impact on the oocyte, we removed the cumulus cells from the gamete following IVM and analyzed the resulting denuded germ cells (Figure 6C). The morphology of the cells was indistinguishable between TMG-treated and untreated controls, and MII eggs with visible polar bodies were observed in both experimental cohorts (Figure 6C). Consistent with what was observed in

intact COCs, isolated gametes showed a dramatic increase in O-GlcNAcylated proteins following TMG treatment (Figure 6D). Taken together, these findings demonstrate that TMG treatment of intact COCs increases O-GlcNAcylated substrates in both the cumulus cells and the germ cell.

Perturbation of O-GlcNAc cycling during meiotic maturation impacts fertilization outcomes but not meiotic progression

To examine whether TMG-induced perturbation of O-GlcNAc cycling impacted meiosis, we scored meiotic progression following IVM in the presence or absence of 50 μM TMG. Because it is difficult to distinguish meiotic stages in bovine gametes solely by transmitted light microscopy due to their high lipid content, we based our scoring on chromatin configuration (Figure 7A). The majority of oocytes in the control and TMG treated groups resumed meiosis, and there was a similar distribution of cells in the various stages of meiosis post-IVM (Figure 7B). Importantly, there was no difference in the percentage of oocytes that reached MII between the experimental cohorts (Figure 7B).

Although an increase in O-GlcNAcylation during IVM does not impair meiotic progression, we wanted to examine whether this treatment could impact the fertilization ability of these cells. Therefore, we performed IVF of bovine COCs following IVM in the presence or absence of 50 03BCM TMG. Maturation in the presence of TMG resulted in a decrease in sperm penetration but also a decrease in the incidence of monospermy (Table 1) (Figure 8). Only 63.93 ± 3.6% of gametes exposed to TMG during IVM resulted in monospermic zygotes compared to 83.08 ± 2.7% of controls (Table 1). In fact, zygotes derived from TMG-treated gametes had an average of 2.48 ± 0.3 sperm per oocyte compared to 1.41 ± 0.1 sperm per oocyte in controls (Table 1)(Figure 8). As is shown in the histogram in Figure 8E, there were fewer monospermic zygotes derived from TMG-treated oocytes relative to controls, and in all instances of polyspermy, there was a higher frequency of TMG-treated oocytes. In the control group, the maximum number of spermatozoa per oocyte was 4 whereas in the TMG group there several cases with more than 10 spermatozoa per oocyte. The ability of a zygote to decondense sperm heads is limited by the cytoplasmic volume (Wolf et al. 1997). DNA from some of the spermatozoa will fully decondense and reach the pronuclear stage while the other sperm heads will remain in either a partially decondensed or compacted stage. Zygotes in both experimental cohorts formed a similar number of male pronuclei per oocyte (1.16±0.03 and 1.17±0.04 male pronuclei/oocyte in the control and TMG groups, respectively) (Table 1). However, the zygotes derived from oocytes matured in TMG had a compromised ability to fully decondense the additional sperm that had penetrated the egg (Figure 8). On average, the TMG cohort had an additional 1.30 ± 0.3 partially decondensed sperm heads per zygote relative to the control cohort that only had 0.24 ± 0.14 (Table 1). Because of this increased number of partially decondensed or compacted sperm heads in the TMG cohort, the overall rate of MPNf based on the number of penetrated oocytes was significantly lower relative to controls (92.35 ± 2.0% vs. 99.00 ± 0.7%, Table 1). Taken together, these findings demonstrate that TMG exposure during IVM has a multi-factorial impact on fertilization with effects on sperm penetration, polyspermy, sperm head decondensation, and pronuclear formation. As a result, TMG treatment reduced the overall output of the IVF system; specifically, only 56.93 ± 3.5% of

oocytes inseminated following IVM in TMG developed into zygotes with 2 pronuclei compared to 80.68 ± 2.8% of the controls (Table 1). Thus, O-GlcNAc homeostasis in the oocyte established during meiotic maturation is required for proper fertilization and zygote development.

Discussion

In this study, the dynamics and localization of O-GlcNAcylation and its modifying enzymes were examined in bovine and human oocytes, which share extensive similarities with respect to patterns of folliculogenesis, endocrinology and gamete morphology. Both bovine and human oocytes expressed the enzymes that regulate O-GlcNAcylation as well as proteins modified with O-GlcNAc. O-GlcNAcylated proteins were found throughout the nucleus and cytoplasm in prophase I-arrested oocytes, and the nuclear envelope clearly contained extensively modified proteins. This localization has been reported in several other cell types, including mouse oocytes and is consistent with nuclear pore complex (NPC) proteins as known substrates of O-GlcNAcylation (Eustice et al. 2017; Zhu et al. 2016). In MII arrested eggs, O-GlcNAcylated substrates are more evenly distributed throughout the cytoplasm with a slight enrichment in the cortex. Interestingly, both OGT and OGA are found in the oocyte cytoplasm but also have distinct subcellular localizations that may reflect unique functions. OGT consistently localized to the meiotic spindles in both bovine and human gametes, and this is consistent with enrichment of OGT at the MI and MII spindles in the mouse oocyte as well as the mitotic spindle in somatic cells (Slawson and Duncan 2015; Slawson et al. 2005). This localization is consistent with the observations that O-GlcNAc cycling plays a critical role in regulating mitotic chromatin dynamics and that O-GlcNAc sites have been mapped on several spindle-associated proteins (Lanza et al. 2016; Slawson et al. 2005; Tan et al. 2013; Tan et al. 2017a; Wang et al. 2010). OGA was enriched at the cortex in bovine and human oocytes across meiosis, and this was also documented in the mouse oocyte (Slawson and Duncan 2015). Because OGT and OGA, which have opposing functions, are concentrated in distinct regions of the oocyte (i.e. spindle vs. cortex), it is tempting to speculate that OGT catalyzes O-GlcNAcylation of spindle proteins during meiosis, whereas OGA expression is minimal at the spindle to limit counteracting OGT activity. Future proteomics studies are needed to identity the specific proteins that are O-GlcNAcylated in the oocyte and to map the modified sites. Although possible, performing mass spectrometry of O-GlcNAcylated substrates is challenging especially in samples that are limited in quantity (Wang et al. 2010).

Although we observed many parallels between bovine and human oocytes with respect to O-GlcNAcylation, there were some differences. For example, the cortical enrichment of O-GlcNAcylated substrates and OGA was more prominent in bovine oocytes relative to human. Moreover, there appeared to be significantly lower levels of O-GlcNAcylated proteins in the human oocytes as it was much more difficult to detect this modification via western blot. These observations may reflect underlying biological differences across species, but it should also be noted that the human eggs used for this research were immature at the time of retrieval and thus not of optimal quality. Despite this inherent limitation of performing research with this source of human oocytes, our data convincingly demonstrate that O-GlcNAc is a highly conserved PTM in mammalian gametes.

In Xenopus oocytes, perturbation of O-GlcNAc cycling perturbs meiotic maturation kinetics (Lefebvre et al. 2004; Slawson et al. 2002). In addition, when O-GlcNAc levels are disrupted in somatic cells, mitotic errors and spindle defects occur (Lanza et al. 2016; Tan et al. 2013). Despite the distinct localization of OGT at the meiotic spindle together with the known role of O-GlcNAc in cell cycle and mitotic spindle regulation, TMG treatment did not overtly impact meiotic progression in bovine oocytes. These findings suggest that oocytes can tolerate significant increases in O-GlcNAcylation during meiotic maturation, but whether they are as tolerant of decreases remains to be investigated. Furthermore, the possibilities that TMG treatment cause subtle alterations in meiotic maturation kinetics or chromosome segregation errors cannot be excluded. Our IVF results, however, suggest that elevated levels of O-GlcNAcylation in the bovine COC during meiotic maturation compromise fertilization and early preimplantation embryo development, with a significant reduction in the percentage of normal zygotes resulting from COCs matured in the presence of TMG.

The findings we observed with TMG are similar to those reported when bovine embryos are matured in medium supplemented with glucosamine and then fertilized (Sutton-McDowall et al. 2006). Neither TMG or glucosamine treatment affects meiotic progression and nuclear maturation, but they do impact preimplantation embryo development (Sutton-McDowall et al. 2006). However, TMG treatment results in an early phenotype at the zygote stage, whereas glucosamine has a later effect on blastocyst development (Sutton-McDowall et al. 2006). The less severe phenotype observed with glucosamine could be because this treatment appears to only increase O-GlcNAcylation in the cumulus cells and not the oocyte (Sutton-McDowall et al. 2006). In contrast, TMG treatment increased O-GlcNAcylation in both the germ and somatic compartments of the COC. Alternatively, it is possible that TMG and glucosamine are acting through different mechanisms, since glucosamine perturbs the HBP upstream of TMG. TMG was synthesized based on rational design and has been used extensively with the express purpose inhibiting OGA with minimal off target effects (de Queiroz et al. 2016; McGreal et al. 2018; Tan et al. 2013; Yuzwa et al. 2008; Zhang et al. 2016; Zhang et al. 2018).

The major phenotypes we observed following IVF of COCs matured in TMG included polyspermy and failure of proper sperm head decondensation. In mammals, the block to polyspermy in the egg is triggered by the calcium-dependent release of cortical granules that contain proteases and zinc that modify the zona pellucida (Que et al. 2017; Tokuhiro and Dean 2018). The calcium that induces these events is released from intracellular stores in the egg in response to IP3 generated from sperm-derived phospholipase Cζ(Ito et al. 2011; Swann and Lai 2016). Interestingly, in some cell lines, the IP3 receptor is regulated by O-GlcNAcylation, so it is possible that this PTM regulates calcium signaling in mammalian eggs as well (Bimboese et al. 2011; Rengifo et al. 2007). Following fertilization, factors within the egg cytoplasm contribute to sperm head decondensation (Caglar et al. 2005). In particular, glutathione present in the egg is a thiol-reducing agent that reduces the protamine disulfide bonds in the first steps of sperm DNA decondensation (Caglar et al. 2005). Interestingly, induction of O-GlcNAcylation results in dysregulation of hepatic glutathione replenishment in a model of acetaminophen-induced liver injury (McGreal et al. 2018). Thus, it is possible that meiotic maturation in the presence of TMG affects glutathione levels in the oocyte, which may have downstream consequences in the zygote on sperm head

decondensation. Interestingly, it is well known in the bovine model that a suboptimal ooplasmic environment fails to induce sperm head decondensation following ICSI (Aguila et al. 2017). Thus, the failure of sperm head decondensation that we observed underscores the poor cytoplasmic environment associated with high O-GlcNAc levels. The specific mechanisms by which O-GlcNAcylation alterations in the oocyte regulates subsequent preimplantation embryo development warrant further investigation and are active research areas.

Conclusions

O-GlcNAcylation is a conserved PTM in the mammalian oocyte that has now been documented in mouse, bovine, and human species (Slawson and Duncan 2015). When O-GlcNAc homeostasis is perturbed during in vitro maturation in bovine COCs, meiotic progression occurs normally. However, when gametes with elevated O-GlcNAcylation are fertilized, zygote development is compromised due to specific effects on the block to polyspermy and sperm head decondensation. It is, therefore, likely that alterations in O-GlcNAcylation will impact fertility in both humans and agricultural species. Ultimately, because the O-GlcNAc modification responds to changes in the metabolic environment and acts as a nutrient sensor, it may serve as a novel marker of gamete quality and source for therapeutic intervention. Moreover, our findings have implications for conditions such as diabetes, obesity, and aging which have a dual impact on O-GlcNAcylation and oocyte quality (Banerjee et al. 2016; Cimadomo et al. 2018; Olivier-Van Stichelen and Hanover 2015; Peterson and Hart 2016; Purcell and Moley 2011; Wang and Moley 2010).

Supplementary Material

Refer to Web version on PubMed Central for supplementary material.

Acknowledgements

We acknowledge Megan Connolly, Rafael Confino, Sarah Wagner, and Dr. Atsuko Kusuhara for technical assistance. We also thank Dr. Jessica E. Hornick for critical insights and discussions about this work. We are also grateful to Dr. T. Rajendra Kumar and the Makowski Family for their recognition of this research.

Funding

This research was supported by: the Master of Science in Reproductive Science and Medicine Program (MS-RSM) at Northwestern University as well as startup funds from the Department of Obstetrics and Gynecology (to F.E.D), the National Institute of Diabetes and Digestive and Kidney Diseases (R01DK100595 to C.S.), the National Cancer Institute (R03CA223949 to C.S.), the AGL2015–66341-R from the Ministry of Economy and Competitiveness (Spain), and the 20040/GERM/16 from Seneca Foundation.

References

Aguila L, Felmer R, Arias ME, Navarrete F, Martin-Hidalgo D, Lee HC, Visconti P, Fissore R. 2017 Defective sperm head decondensation undermines the success of ICSI in the bovine. Reproduction 154(3):307–318. [PubMed: 28751536]

Alonso J, Schimpl M, van Aalten DM. 2014 O-GlcNAcase: promiscuous hexosaminidase or key regulator of O-GlcNAc signaling? The Journal of biological chemistry 289(50):34433–34439. [PubMed: 25336650]

Banerjee PS, Lagerlof O, Hart GW. 2016 Roles of O-GlcNAc in chronic diseases of aging. Mol Aspects Med 51:1–15. [PubMed: 27259471]

Bimboese P, Gibson CJ, Schmidt S, Xiang W, Ehrlich BE. 2011 Isoform-specific regulation of the inositol 1,4,5-trisphosphate receptor by O-linked glycosylation. The Journal of biological chemistry 286(18):15688–15697. [PubMed: 21383013]

Bond MR, Hanover JA. 2015 A little sugar goes a long way: the cell biology of O-GlcNAc. J Cell Biol 208(7):869–880. [PubMed: 25825515]

Caglar GS, Hammadeh M, Asimakopoulos B, Nikolettos N, Diedrich K, Al-Hassani S. 2005 In vivo and in vitro decondensation of human sperm and assisted reproduction technologies. In Vivo 19(3): 623–630. [PubMed: 15875785]

Cimadomo D, Fabozzi G, Vaiarelli A, Ubaldi N, Ubaldi FM, Rienzi L. 2018 Impact of Maternal Age on Oocyte and Embryo Competence. Front Endocrinol (Lausanne) 9:327. [PubMed: 30008696]

de Queiroz RM, Madan R, Chien J, Dias WB, Slawson C. 2016 Changes in O-Linked N-Acetylglucosamine (O-GlcNAc) Homeostasis Activate the p53 Pathway in Ovarian Cancer Cells. The Journal of biological chemistry 291(36):18897–18914. [PubMed: 27402830]

Dumesic DA, Padmanabhan V, Abbott DH. 2008 Polycystic ovary syndrome and oocyte developmental competence. Obstet Gynecol Surv 63(1):39–48. [PubMed: 18081939]

Eppig JJ, Pendola FL, Wigglesworth K, Pendola JK. 2005 Mouse oocytes regulate metabolic cooperativity between granulosa cells and oocytes: amino acid transport. Biol Reprod 73(2):351–357. [PubMed: 15843493]

Eustice M, Bond MR, Hanover JA. 2017 O-GlcNAc cycling and the regulation of nucleocytoplasmic dynamics. Biochemical Society transactions 45(2):427–436. [PubMed: 28408483]

Frank LA, Sutton-McDowall ML, Brown HM, Russell DL, Gilchrist RB, Thompson JG. 2014a Hyperglycaemic conditions perturb mouse oocyte in vitro developmental competence via beta-O-linked glycosylation of heat shock protein 90. Hum Reprod 29(6):1292–1303. [PubMed: 24713123]

Frank LA, Sutton-McDowall ML, Gilchrist RB, Thompson JG. 2014b The effect of peri-conception hyperglycaemia and the involvement of the hexosamine biosynthesis pathway in mediating oocyte and embryo developmental competence. Mol Reprod Dev 81(5):391–408. [PubMed: 24415135]

Gosden R, Lee B. 2010 Portrait of an oocyte: our obscure origin. J Clin Invest 120(4):973–983. [PubMed: 20364095]

Gu L, Liu H, Gu X, Boots C, Moley KH, Wang Q. 2015 Metabolic control of oocyte development: linking maternal nutrition and reproductive outcomes. Cell Mol Life Sci 72(2):251–271. [PubMed: 25280482]

Hardiville S, Hart GW. 2014 Nutrient regulation of signaling, transcription, and cell physiology by O-GlcNAcylation. Cell metabolism 20(2):208–213. [PubMed: 25100062]

Hart GW. 2014 Three Decades of Research on O-GlcNAcylation - A Major Nutrient Sensor That Regulates Signaling, Transcription and Cellular Metabolism. Front Endocrinol (Lausanne) 5:183. [PubMed: 25386167]

Ito J, Parrington J, Fissore RA. 2011 PLCzeta and its role as a trigger of development in vertebrates. Mol Reprod Dev 78(10–11):846–853. [PubMed: 21823187]

Janetzko J, Walker S. 2014 The making of a sweet modification: structure and function of O-GlcNAc transferase. The Journal of biological chemistry 289(50):34424–34432. [PubMed: 25336649]

Lanza C, Tan EP, Zhang Z, Machacek M, Brinker AE, Azuma M, Slawson C. 2016 Reduced O-GlcNAcase expression promotes mitotic errors and spindle defects. Cell cycle 15(10):1363–1375. [PubMed: 27070276]

Lefebvre T, Baert F, Bodart JF, Flament S, Michalski JC, Vilain JP. 2004 Modulation of O-GlcNAc glycosylation during Xenopus oocyte maturation. Journal of cellular biochemistry 93(5):999–1010. [PubMed: 15389870]

McGreal SR, Bhushan B, Walesky C, McGill MR, Lebofsky M, Kandel SE, Winefield RD, Jaeschke H, Zachara NE, Zhang Z, Tan EP, Slawson C, Apte U. 2018 Modulation of O-GlcNAc Levels in the Liver Impacts Acetaminophen-Induced Liver Injury by Affecting Protein Adduct Formation and Glutathione Synthesis. Toxicol Sci 162(2):599–610. [PubMed: 29325178]

Mondejar I, Grullon LA, Garcia-Vazquez FA, Romar R, Coy P. 2012 Fertilization outcome could be regulated by binding of oviductal plasminogen to oocytes and by releasing of plasminogen activators during interplay between gametes. Fertility and sterility 97(2):453–461. [PubMed: 22177313]

Olivier-Van Stichelen S, Hanover JA. 2015 You are what you eat: O-linked N-acetylglucosamine in disease, development and epigenetics. Curr Opin Clin Nutr Metab Care 18(4):339–345. [PubMed: 26049631]

Pantaleon M, Tan HY, Kafer GR, Kaye PL. 2010 Toxic effects of hyperglycemia are mediated by the hexosamine signaling pathway and o-linked glycosylation in early mouse embryos. Biol Reprod 82(4):751–758. [PubMed: 20032283]

Parrish JJ, Susko-Parrish J, Winer MA, First NL. 1988 Capacitation of bovine sperm by heparin. Biol Reprod 38(5):1171–1180. [PubMed: 3408784]

Peterson SB, Hart GW. 2016 New insights: A role for O-GlcNAcylation in diabetic complications. Crit Rev Biochem Mol Biol 51(3):150–161. [PubMed: 26806492]

Purcell SH, Moley KH. 2011 The impact of obesity on egg quality. J Assist Reprod Genet 28(6):517–524. [PubMed: 21625966]

Que EL, Duncan FE, Bayer AR, Philips SJ, Roth EW, Bleher R, Gleber SC, Vogt S, Woodruff TK, O'Halloran TV. 2017 Zinc sparks induce physiochemical changes in the egg zona pellucida that prevent polyspermy. Integr Biol (Camb) 9(2):135–144. [PubMed: 28102396]

Rengifo J, Gibson CJ, Winkler E, Collin T, Ehrlich BE. 2007 Regulation of the inositol 1,4,5-trisphosphate receptor type I by O-GlcNAc glycosylation. J Neurosci 27(50):13813–13821. [PubMed: 18077693]

Russell DL, Gilchrist RB, Brown HM, Thompson JG. 2016 Bidirectional communication between cumulus cells and the oocyte: Old hands and new players? Theriogenology 86(1):62–68. [PubMed: 27160446]

Slawson C, Duncan FE. 2015 Sweet action: The dynamics of O-GlcNAcylation during meiosis in mouse oocytes. Mol Reprod Dev 82(12):915. [PubMed: 26331270]

Slawson C, Lakshmanan T, Knapp S, Hart GW. 2008 A mitotic GlcNAcylation/phosphorylation signaling complex alters the posttranslational state of the cytoskeletal protein vimentin. Mol Biol Cell 19(10):4130–4140. [PubMed: 18653473]

Slawson C, Shafii S, Amburgey J, Potter R. 2002 Characterization of the O-GlcNAc protein modification in Xenopus laevis oocyte during oogenesis and progesterone-stimulated maturation. Biochimica et biophysica acta 1573(2):121–129. [PubMed: 12399021]

Slawson C, Zachara NE, Vosseller K, Cheung WD, Lane MD, Hart GW. 2005 Perturbations in O-linked beta-N-acetylglucosamine protein modification cause severe defects in mitotic progression and cytokinesis. The Journal of biological chemistry 280(38):32944–32956. [PubMed: 16027160]

Sutton-McDowall ML, Mitchell M, Cetica P, Dalvit G, Pantaleon M, Lane M, Gilchrist RB, Thompson JG. 2006 Glucosamine supplementation during in vitro maturation inhibits subsequent embryo development: possible role of the hexosamine pathway as a regulator of developmental competence. Biol Reprod 74(5):881–888. [PubMed: 16436527]

Swann K, Lai FA. 2016 The sperm phospholipase C-zeta and Ca2+ signalling at fertilization in mammals. Biochemical Society transactions 44(1):267–272. [PubMed: 26862214]

Tan EP, Caro S, Potnis A, Lanza C, Slawson C. 2013 O-linked N-acetylglucosamine cycling regulates mitotic spindle organization. The Journal of biological chemistry 288(38):27085–27099. [PubMed: 23946484]

Tan EP, Duncan FE, Slawson C. 2017a The sweet side of the cell cycle. Biochemical Society transactions 45(2):313–322. [PubMed: 28408472]

Tan EP, McGreal SR, Graw S, Tessman R, Koppel SJ, Dhakal P, Zhang Z, Machacek M, Zachara NE, Koestler DC, Peterson KR, Thyfault JP, Swerdlow RH, Krishnamurthy P, DiTacchio L, Apte U, Slawson C. 2017b Sustained O-GlcNAcylation reprograms mitochondrial function to regulate energy metabolism. The Journal of biological chemistry 292(36):14940–14962. [PubMed: 28739801]

Tokuhiro K, Dean J. 2018 Glycan-Independent Gamete Recognition Triggers Egg Zinc Sparks and ZP2 Cleavage to Prevent Polyspermy. Dev Cell 46(5):627–640 e625. [PubMed: 30122633]

Wang Q, Moley KH. 2010 Maternal diabetes and oocyte quality. Mitochondrion 10(5):403–410. [PubMed: 20226883]

Wang Z, Udeshi ND, Slawson C, Compton PD, Sakabe K, Cheung WD, Shabanowitz J, Hunt DF, Hart GW. 2010 Extensive crosstalk between O-GlcNAcylation and phosphorylation regulates cytokinesis. Science signaling 3(104):ra2. [PubMed: 20068230]

Ward F, Enright B, Rizos D, Boland M, Lonergan P. 2002 Optimization of in vitro bovine embryo production: effect of duration of maturation, length of gamete co-incubation, sperm concentration and sire. Theriogenology 57(8):2105–2117. [PubMed: 12066869]

Wolf JP, Ducot B, Aymar C, Rodrigues D, Desjardin S, Jardin A, Jouannet P. 1997 Absence of block to polyspermy at the human oolemma. Fertility and sterility 67(6):1095–1102. [PubMed: 9176450]

Wong SL, Wu LL, Robker RL, Thompson JG, McDowall ML. 2015 Hyperglycaemia and lipid differentially impair mouse oocyte developmental competence. Reprod Fertil Dev 27(4):583–592. [PubMed: 25714624]

Yuzwa SA, Macauley MS, Heinonen JE, Shan X, Dennis RJ, He Y, Whitworth GE, Stubbs KA, McEachern EJ, Davies GJ, Vocadlo DJ. 2008 A potent mechanism-inspired O-GlcNAcase inhibitor that blocks phosphorylation of tau in vivo. Nat Chem Biol 4(8):483–490. [PubMed: 18587388]

Zhang Z, Costa FC, Tan EP, Bushue N, DiTacchio L, Costello CE, McComb ME, Whelan SA, Peterson KR, Slawson C. 2016 O-Linked N-Acetylglucosamine (O-GlcNAc) Transferase and O-GlcNAcase Interact with Mi2beta Protein at the Agamma-Globin Promoter. The Journal of biological chemistry 291(30):15628–15640. [PubMed: 27231347]

Zhang Z, Parker MP, Graw S, Novikova LV, Fedosyuk H, Fontes JD, Koestler DC, Peterson KR, Slawson C. 2018 O-GlcNAc homeostasis contributes to cell fate decisions during hematopoiesis. The Journal of biological chemistry.

Zhang Z, Tan EP, VandenHull NJ, Peterson KR, Slawson C. 2014 O-GlcNAcase Expression is Sensitive to Changes in O-GlcNAc Homeostasis. Front Endocrinol (Lausanne) 5:206. [PubMed: 25520704]

Zhu Y, Liu TW, Madden Z, Yuzwa SA, Murray K, Cecioni S, Zachara N, Vocadlo DJ. 2016 Post-translational O-GlcNAcylation is essential for nuclear pore integrity and maintenance of the pore selectivity filter. J Mol Cell Biol 8(1):2–16. [PubMed: 26031751]

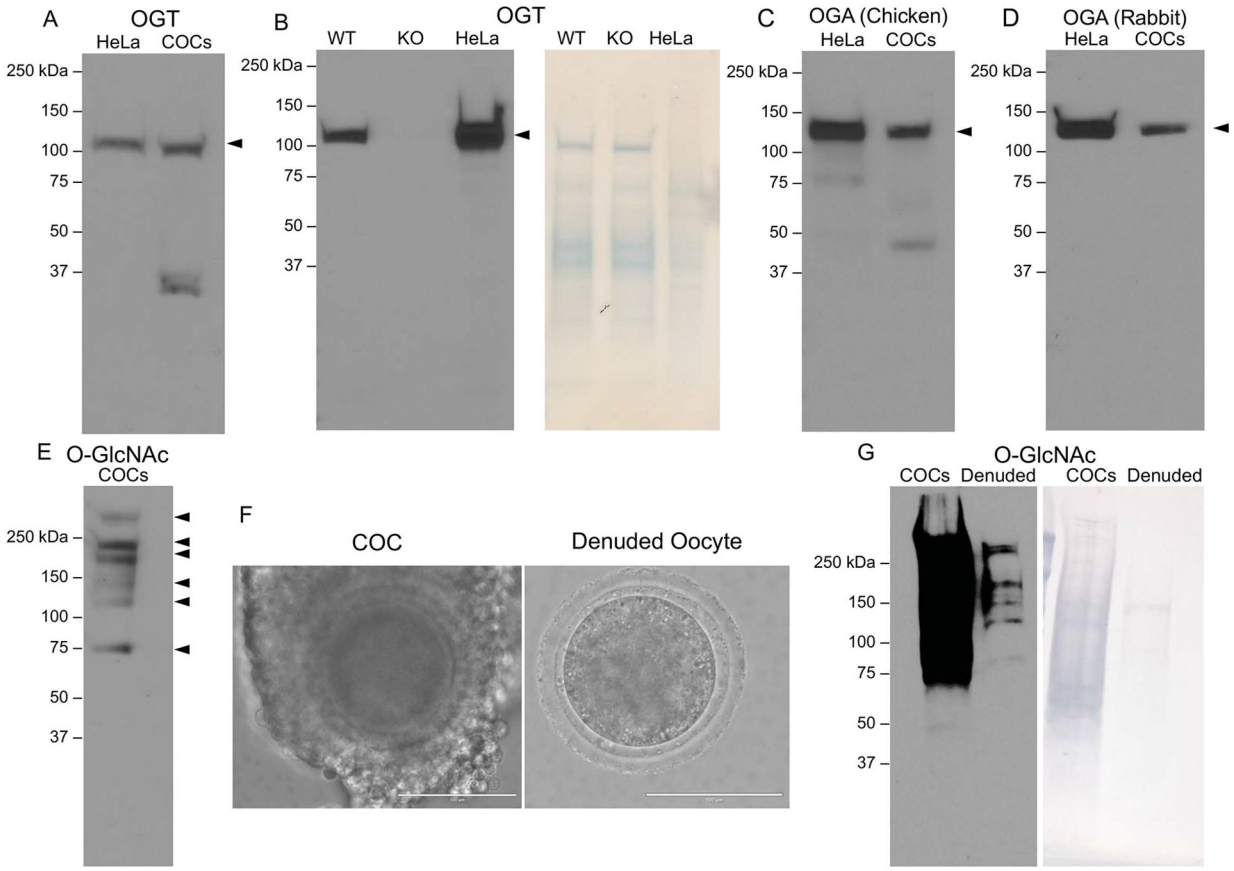

Figure 1. Enzymes that regulate O-GlcNAcylation and O-GlcNAcylated substrates are expressed in bovine cumulus oocyte complexes.

Protein extracts from bovine cumulus oocyte complexes (COC) were processed for immunoblot analysis and probed with antibodies against (A–B) OGT (C) OGA (polyclonal antibody raised in chicken), (D) OGA (polyclonal antibody raised in rabbit), and (E) the O-GlcNAc modification. Where relevant, 25 μg of HeLa cell lysate, wildtype mouse liver extract, and knockout mouse liver extract were used as controls. (F) Representative images of COCs and denuded oocytes used for immunoblots in (G) are shown (scale bars are 100 μm). (G) Immunoblot comparing O-GlcNAc levels in protein extracts from bovine COCs and denuded oocytes. In (B) and (G), SWIFT staining was performed to detect total protein and confirm equal loading per lane. All immunoblots were repeated at least three times with 15 COCs and 15 denuded oocytes loaded per lane and representative images are shown.

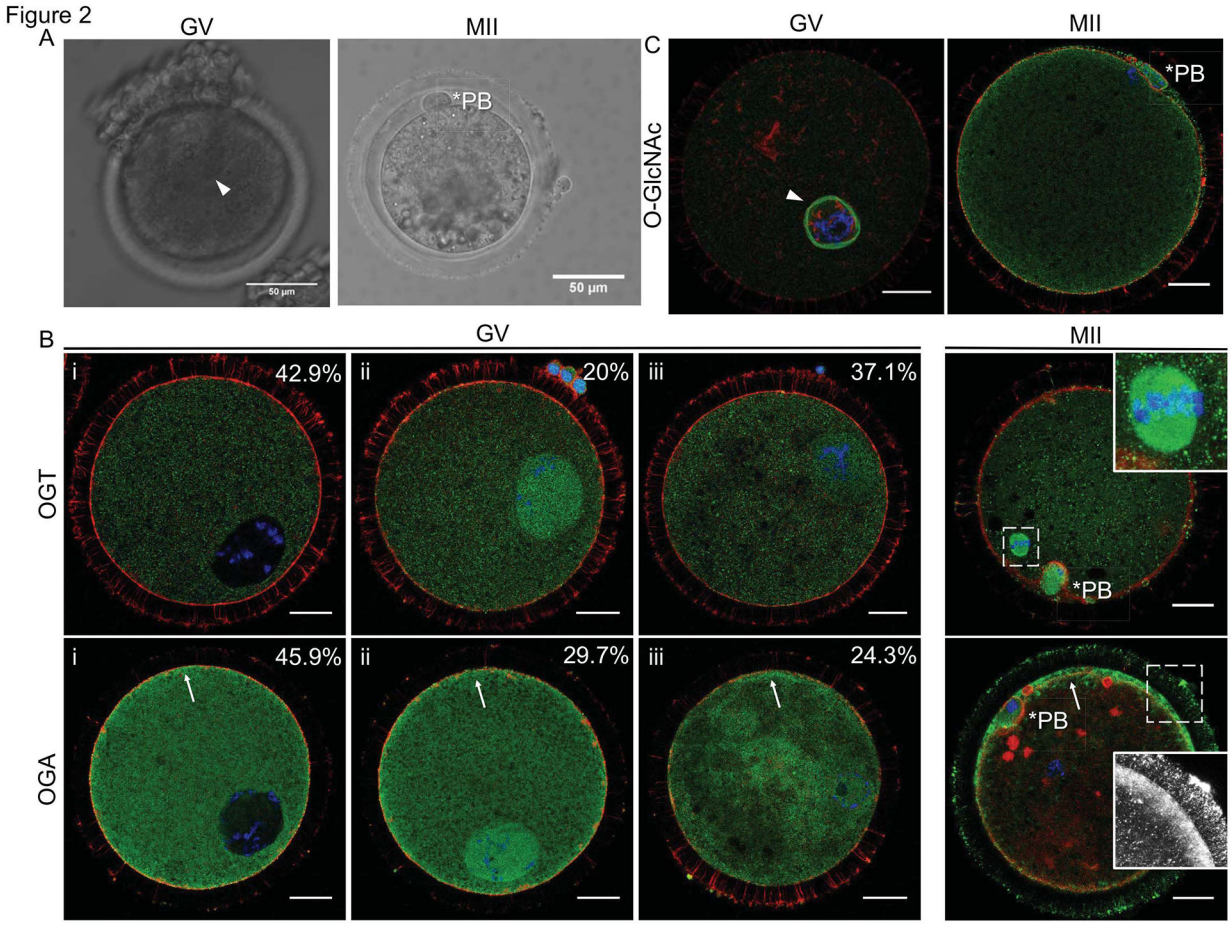

Figure 2. OGA, OGT, and O-GlcNAcylated proteins have dynamic distributions in bovine oocytes during meiotic maturation.

Representative transmitted light images of a GV-intact oocyte and an MII-arrested egg used for immunofluorescence studies. Immunofluorescence and confocal microscopy were performed in GV oocytes and MII-arrested eggs for (B) OGT, OGA, and (C) O-GlcNAc. The distribution of OGA and OGT in GV oocytes was categorized as follows (i) primarily cytoplasmic and excluded from the nucleus, (ii) cytoplasmic and enriched at the nucleus, or (iii) uniformly distributed throughout the cytoplasm and nucleus. The percentage of cells within each category is noted. In MII stage oocytes, the inset in the OGT image highlights the spindle localization, and the inset in the OGA image highlights localization to transzonal projections (note that the red foci of actin in this particular image may be remnants of disrupted transzonal projections or the cumulus cell cytoskeleton and were not consistently observed). The arrowhead marks the GV in (A) and the nuclear envelope in (C), the asterisks mark the polar bodies (PB), and the arrows highlight the enrichment of OGA at the cortex. For all fluorescence images, DNA is shown in blue, F-actin in red, and the marker of interest (OGT, OGA, O-GlcNAc) in green. Single optical sections are shown except for insets where projections are shown. Between 10–60 cells were examined for each marker at each meiotic stage and representative images are shown. The scale bars in (A) are 50 μm and in (B–C) are 25 μm. A projection of the GV oocyte in (C) is shown in Supplemental Figure 2.

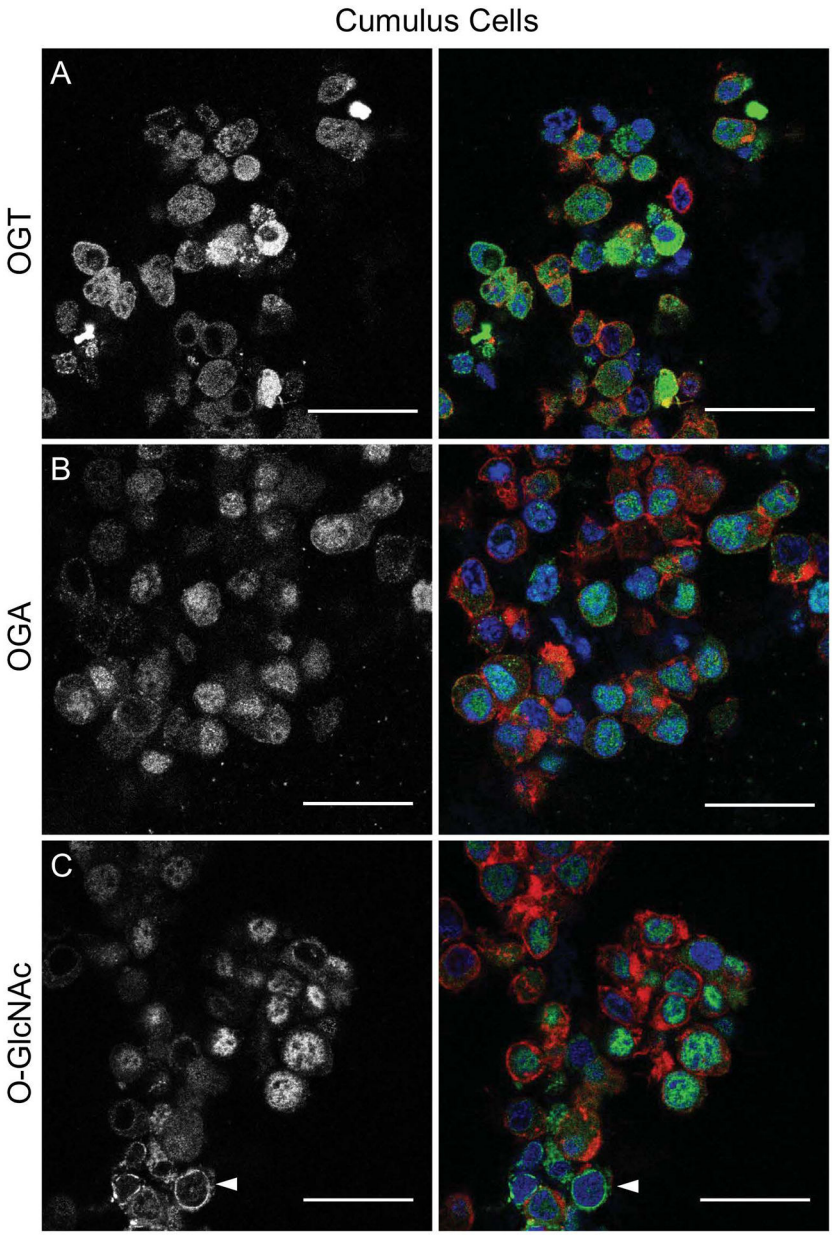

Figure 3. OGA, OGT, and O-GlcNAcylated proteins are expressed in bovine cumulus cells.

Cumulus cells were isolated from bovine COCs collected from antral follicles and analyzed by immunofluorescence and confocal microscopy for (A) OGT, (B) OGA and (C) O-GlcNAc. The gray scale images (left) show the localization of each specific marker, and the merged images (right) show DNA in blue, F-actin in red, and the marker of interest (OGT, OGA, O-GlcNAc) in green. Single optical sections are shown. The arrowhead in (C) highlights O-GlcNAcylated proteins that localize to the nuclear envelope. This experiment was repeated three times with pools of cumulus cells and representative images are shown. The scale bars are 25 μm.

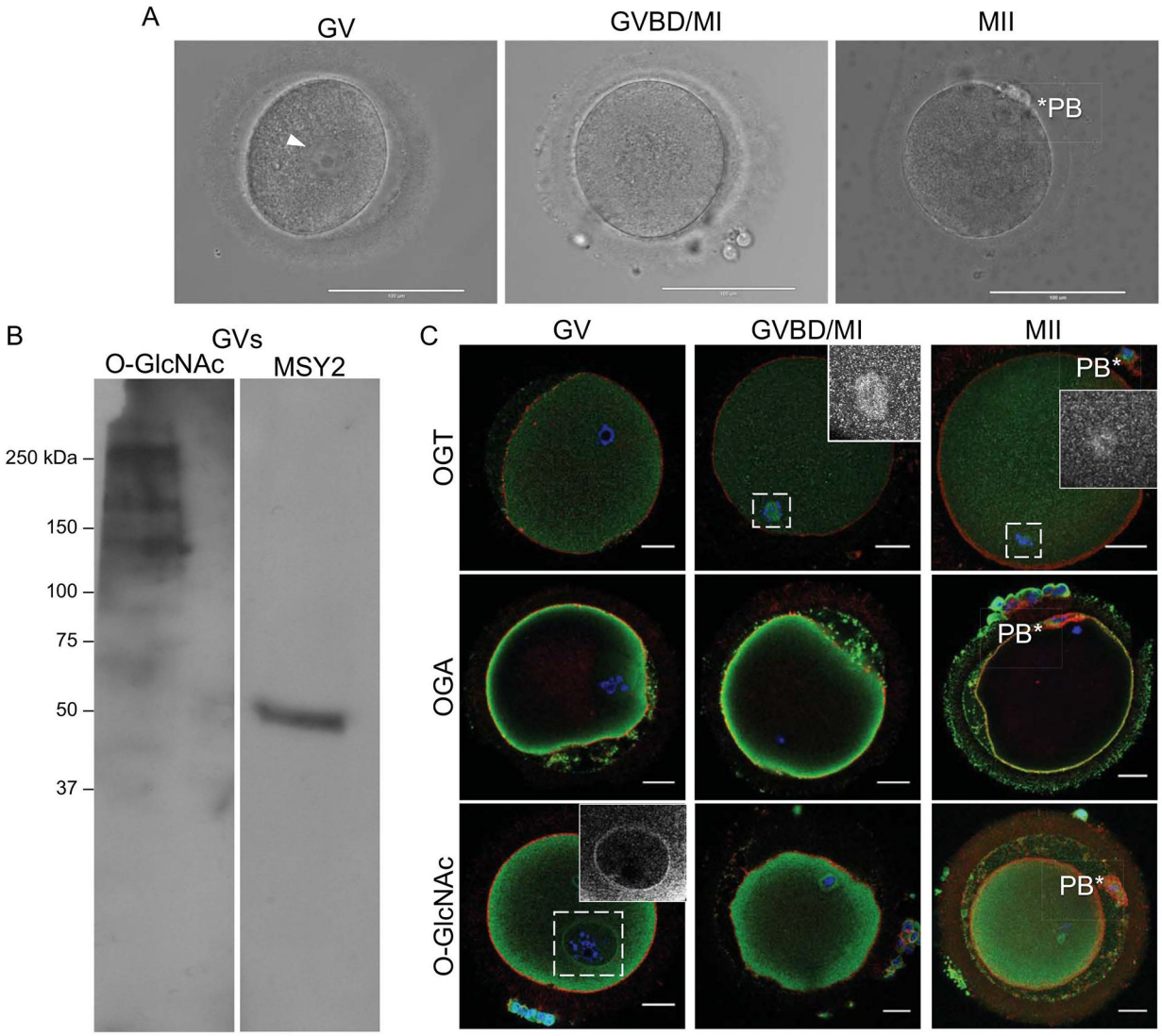

Figure 4. OGA, OGT, and O-GlcNAcylated proteins are expressed in human oocytes.

(A) Representative images of human oocytes distinct stages of meiosis are shown (GV; germinal vesicle intact, GVBD/MI; germinal vesicle breakdown/metaphase of meiosis I, and MII; metaphase of meiosis II). The arrowhead marks the GV, and the asterisks marks the polar body (PB). (B) Immunoblot analysis of protein extracts from human oocytes probed with an antibody against O-GlcNAc and MSY2 to confirm that oocytes were loaded. This was repeated twice with extracts from between 30–35 oocytes loaded per lane, and a representative image is shown. (C) Immunofluorescence and confocal microscopy were performed for OGT, OGA, and O-GlcNAc at the GV, GVBD/MI, and MII stages. In the OGT images, the insets highlight MI and MII spindle localization. In the O-GlcNAc image, the inset highlights the staining at the nuclear envelope. The asterisks mark the polar bodies (PB). For all fluorescence images, DNA is shown in blue, F-actin in red, and the marker of interest (OGT, OGA, O-GlcNAc) in green. Single optical sections are shown except for insets where projections are shown. Between 3–5 cells at each stage of meiosis were

examined for each marker and representative images are shown. The scale bars in (A) are 100 μm and in (C) are 25 μm.

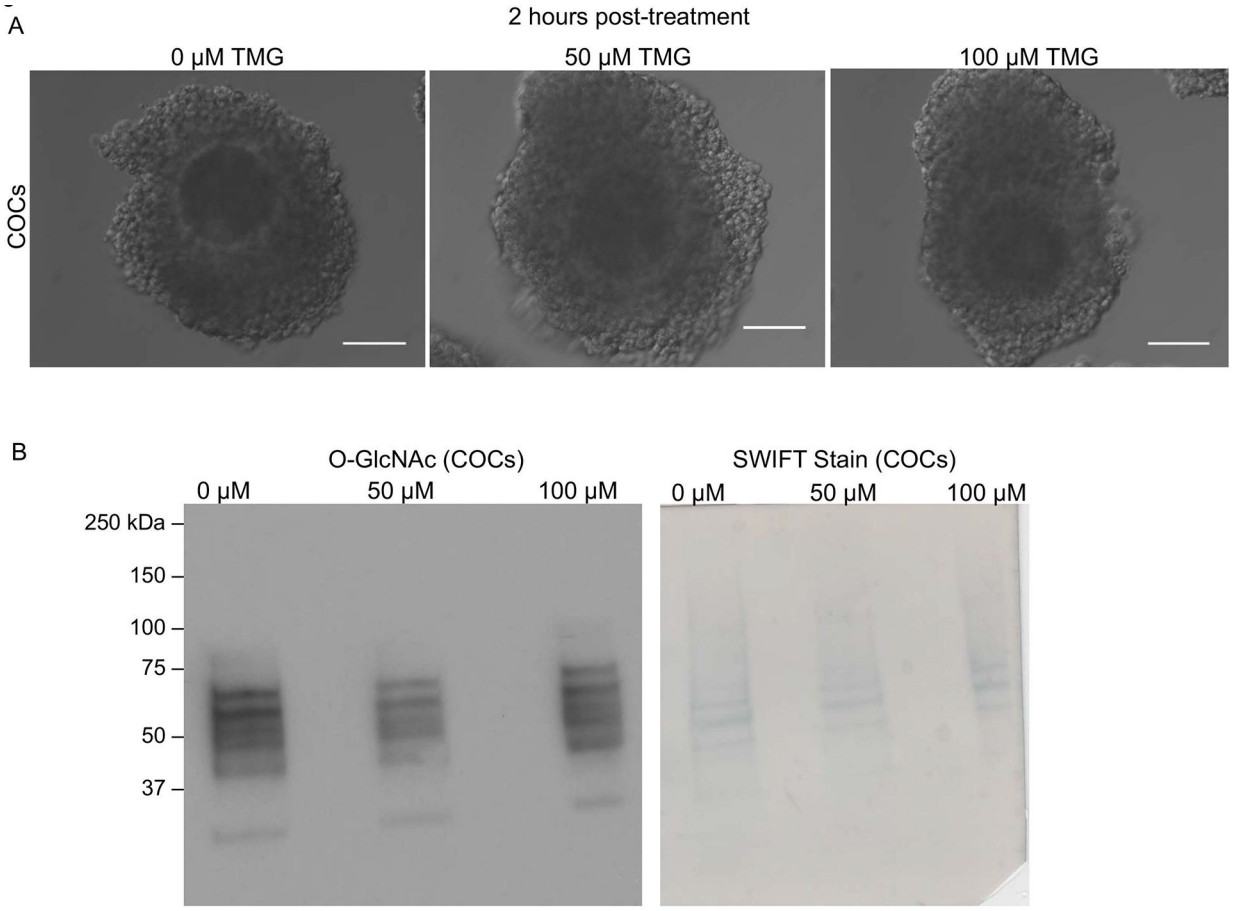

Figure 5. Two-hour TMG treatment does not affect O-GlcNAc levels in bovine COCs.

The morphology of bovine COCs treated with 0 μM, 50 μM, and 100 μM TMG for 2 hours is shown. (B) Immunoblot analysis of O-GlcNAc levels in bovine COCs treated with 0 μM, 50 μM, and 100 μM TMG for 2 hours was performed. Protein extracts from 15 COCs were loaded per lane. Swift staining (right) was used to visualize total protein. This experiment was repeated three times and representative images are shown. The scale bars in (A) are 100 μm.

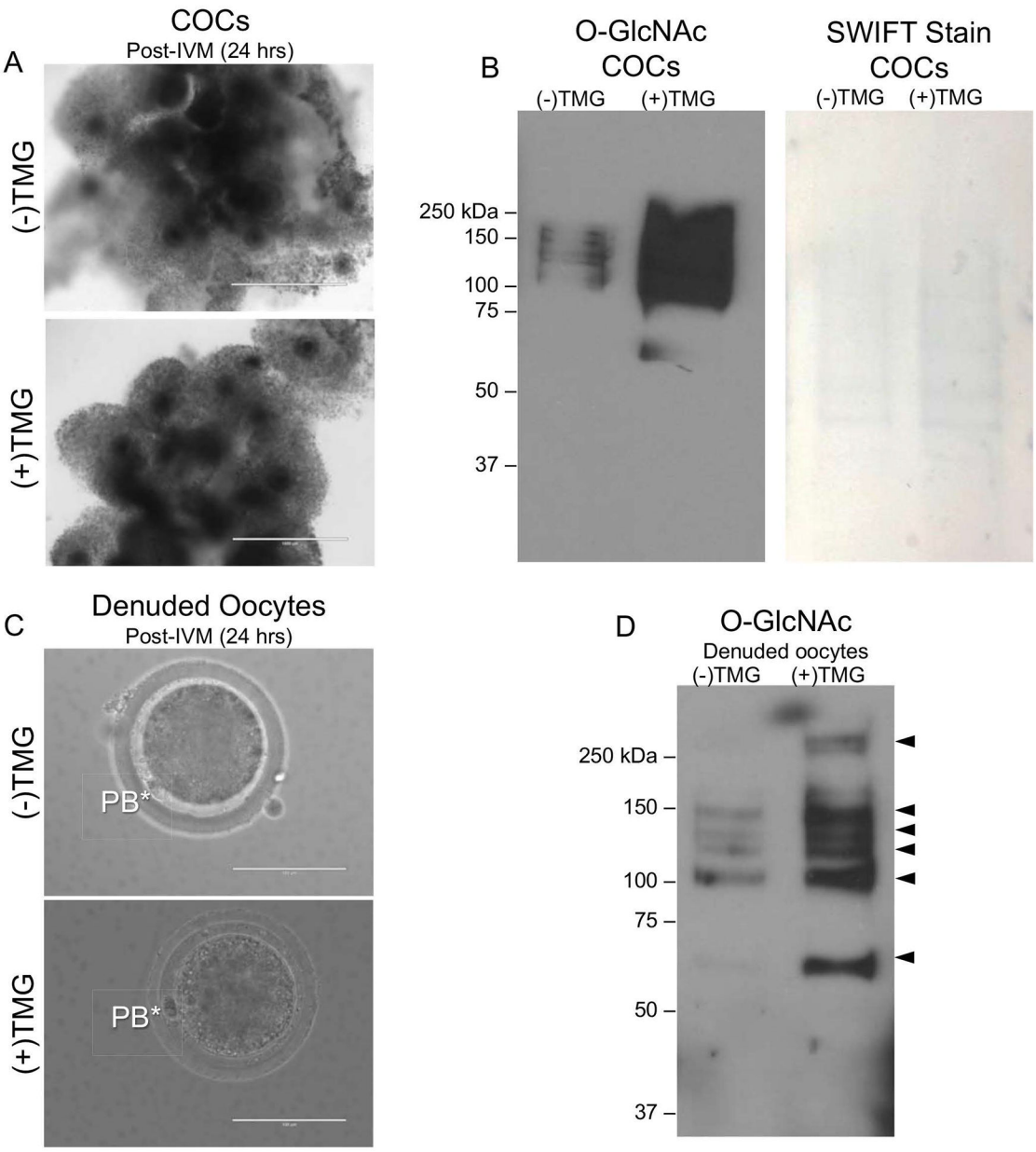

Figure 6. TMG-treatment during in vitro maturation increases O-GlcNAc levels in the bovine COC and oocyte.

(A) Morphology of COCs following +/− treatment with 50 μM TMG for the duration of IVM (24 hours) is shown. Note the equivalent degree of cumulus expansion in both groups. (B) Immunoblot analysis of O-GlcNAc levels in protein extracts from intact bovine COCs treated with 0 μM, and 50 μM for was performed. Protein extracts from 15 COCs were loaded per lane. Swift staining (right) was used to visualize total protein. (C) Representative images of MII eggs isolated from COCs following IVM +/− 50 μM TMG are shown. The asterisks mark the polar bodies (PB). (D) Immunoblot analysis of O-GlcNAc levels in protein extracts from gametes that were stripped from cumulus cells following IVM +/− 50 μM TMG was performed. Protein extracts from equal number of denuded gametes (N = 15)

were loaded per lane. All experiments were repeated three times and representative images are shown. The scale bars in (A) are 1 mm and in (C) are 100 μm.

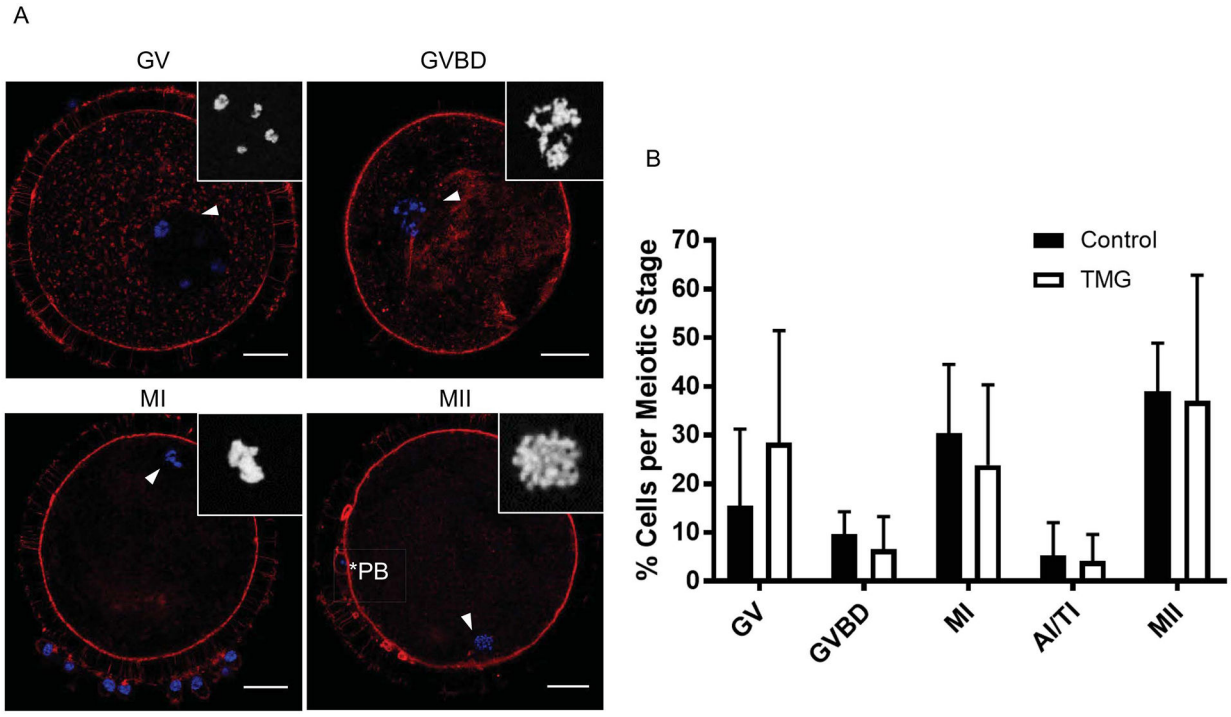

Figure 7. TMG treatment of bovine COCs during in vitro maturation does not impact meiotic progression.

The meiotic stage of oocytes following IVM +/− 50 μM TMG was scored by assessing chromatin configuration via immunostaining and confocal microscopy. (A) Representative images of oocytes at the various meiotic stages are shown (GV; germinal vesicle intact, GVBD; germinal vesicle breakdown, MI; metaphase of meiosis I, and MII; metaphase of meiosis II). DNA is shown in blue and F-actin in red. The arrowhead marks the chromatin that is further magnified in the inset. The asterisks mark the polar body (PB). Single optical sections are shown except for insets where projections are shown. (B) Meiotic progression in each treatment group was plotted and no significant differences were observed. Scale bars in (A) are 25 μm. Meiotic progression data were compiled from nine experimental replicates and included a total of 120 control COCs and 99 TMG-treated COCs.

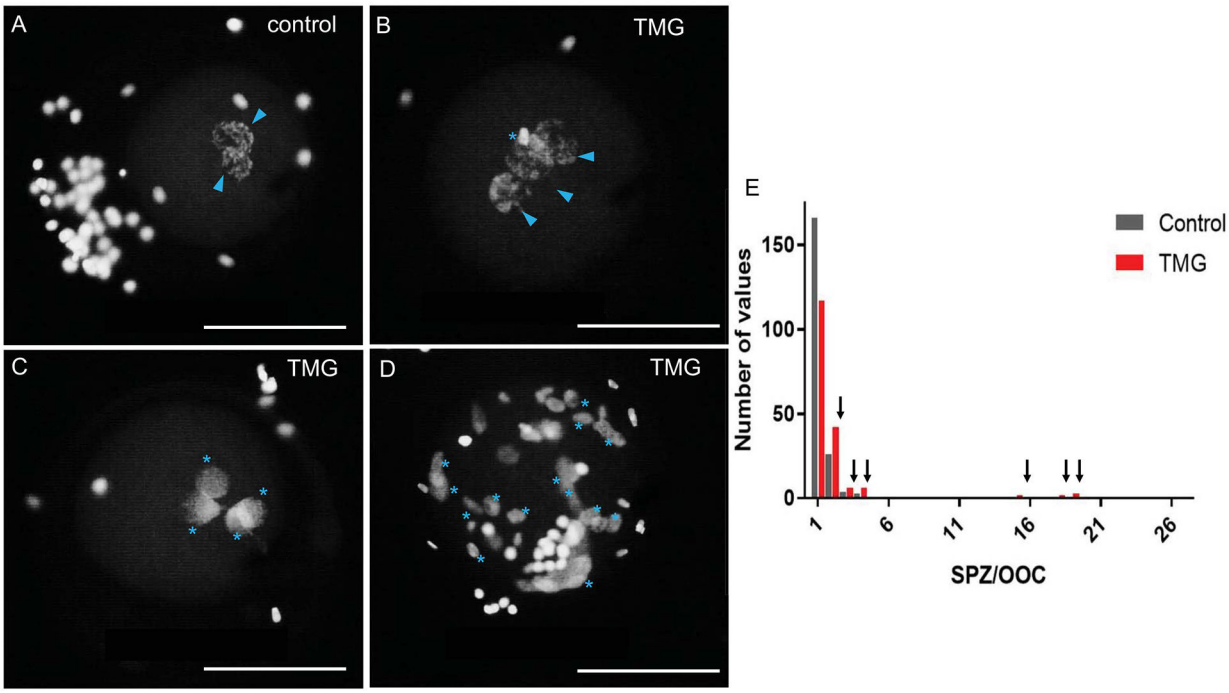

Figure 8. TMG treatment of bovine COCs during in vitro maturation results in zygotic defects.

18 hours post-insemination, zygotes derived from oocytes that were matured +/− 50 μM TMG were fixed to visualize DNA to assess sperm penetration, sperm decondensation, and pronuclear formation. Representative images of (A) control zygotes with two pronuclei and those from (B-D) TMG treatment are shown. The blue arrowheads highlight pronuclei while the blue asterisks highlight multiple sperm in various states of decondensation. The zygote in (D) illustrates an extreme cases of polyspermy. In all images, the nuclei on the outside of the zygote are from lingering cumulus cells. Scale bars are 100 μm. (E) A histogram showing the frequency distribution of the number of spermatozoa per oocyte in zygotes derived from either TMG-treated (red bars) or control oocytes (grey bars). Arrows highlight the increased number of TMG-treated oocytes in all cases of polyspermy. For these experiments, >200 zygotes in each treatment group were analyzed across three replicates.

Table 1.

Fertilization outcomes of bovine oocytes in vitro matured in the presence or absence of 50 μM TMG.

Results were assessed 18 h post insemination. MPNf (male pronuclear formation rate), SPZ/OO (mean number of spermatozoa per penetrated oocyte), MPN (number of male pronucleus in each penetrated oocytes). The data are compiled from three replicates and are expressed as mean ± standard error of the mean (SEM). Different letters in the same column indicate significant differences (P<0.05).

GROUP	N	Penetration (%)	Monospermy* (%)	SPZ/OO*	Decondensed SPZ/OO*	MPN/OO*	MPNf* (%)	Output** (%)
Control	207	97.10 ± 1.17[a]	83.08 ± 2.65[a]	1.41 ± 0.14[a]	0.24 ± 0.14[a]	1.16±0.03	99.00 ± 0.70[a]	80.68 ± 2.75[a]
TMG	202	90.59 ± 2.06[b]	63.93 ± 3.56[b]	2.48 ± 0.32[b]	1.30 ± 0.34[b]	1.17±0.04	92.35 ± 1.97[b]	56.93 ± 3.49[b]
P value		0.0059	<0.001	0.0020	0.0037	0.8456	0.0011	<0.001

*From penetrated oocytes

**Zygotes with 2 pronuclei from total number of inseminated oocytes